

Cite this: *Mater. Horiz.*, 2022, 9, 1309Received 4th December 2021,  
Accepted 7th February 2022

DOI: 10.1039/d1mh01965a

rsc.li/materials-horizons

# Modular penetration and controlled release (MP-CR): improving the internal modification of natural hierarchical materials with smart nanoparticles†

Ruixin Zhu,<sup>‡ab</sup> Junchao Wang,<sup>‡ab</sup> Kaijun Li,<sup>ab</sup> Chaojian Chen<sup>ib</sup>\*<sup>c</sup> and Gongyan Liu<sup>ib</sup>\*<sup>ab</sup>

The internal modification of natural hierarchical materials can largely improve their inherent properties and afford them new functions. However, conventional methods using small-molecule agents often encounter poor uniformity and low efficiency. By comparing the penetration of small molecules and nanoparticles into hierarchical collagen fibers, we propose a general strategy, namely modular penetration and controlled release (MP-CR), for the internal modification of 3D biomass materials. We demonstrate that nano-sized aluminum-loaded particles can penetrate into collagen networks more effectively and evenly than small-molecule crosslinkers. After the on-demand pH-triggered release of interactive aluminum ions, enhanced internal crosslinking is achieved. Importantly, we elucidate the mechanism in depth and show that the MP-CR strategy can comprehensively improve the overall performance of natural hierarchical materials. The MP-CR strategy represents a significant step forward for the internal modification of hierarchical materials, which will find broad applications in biomedicine, catalysis, water treatment, soft electronics, and energy storage.

## 1. Introduction

Three-dimensional ordered architectures from the nanoscale to micro- and macro-scales are ubiquitous in natural biomass materials such as cellulose in plants, chitin and collagen fibers in animals, and silk fibroin from spiders and silkworms.<sup>1–8</sup> Due

### New concepts

We demonstrate a novel strategy, called modular penetration and controlled release (MP-CR), to overcome some major challenges in the internal modification of natural hierarchical materials such as poor uniformity and low efficiency. Unlike conventional strategies based on small molecules, MP-CR uses responsive nanoparticles to deliver and release reactive crosslinkers. We show that nano-sized aluminum particles (Al-NPs) with a relatively larger size can more uniformly and effectively penetrate into hierarchical collagen networks than conventional small-molecule crosslinkers. This surprising and counterintuitive phenomenon has been elucidated through careful investigation of the unique two-step penetration and release process of nanoparticles within collagen networks. Due to the nano-size effect and their inert surface, the Al-NPs only travel into relatively larger pores. After on-demand pH-controlled disassembly, the released crosslinkers further diffuse into nanoscale vacancies between collagen molecules, leading to more effective and even internal crosslinking. Remarkably, the samples treated by the MP-CR strategy reveal comprehensively improved crosslinking uniformity, mechanical properties, and chemical stability. Meanwhile, the environmental pollution in conventional processing can be tremendously reduced. In principle, MP-CR is compatible with different functional nanoparticles, and it should be applicable to reinforce and functionalize other natural and synthetic hierarchical materials for various emerging applications.

to their high porosity and large inner surface areas, these hierarchical structures demonstrate outstanding adsorption and energy storage capabilities, as well as catalytic and thermo-electric properties.<sup>9–13</sup> Therefore, natural biomass materials have attracted great attention for various emerging applications in biomedicine, catalysis, soft electronics, water treatment and energy storage.<sup>14–19</sup> However, these hierarchical materials also present some drawbacks such as poor thermal and chemical stability, which restrict their wider applications.<sup>20</sup> Internal modification of these natural materials can provide vast opportunities to enhance their intrinsic properties and afford them new functions.<sup>21–24</sup> For example, in the leather industry, there has been a long history of treating leather with tanning agents to improve its mechanical strength and softness.

<sup>a</sup> National Engineering Research Center of Clean Technology in Leather Industry, College of Biomass Science and Engineering, Sichuan University, Chengdu 610065, China. E-mail: lgy3506@scu.edu.cn

<sup>b</sup> Key Laboratory of Leather Chemistry and Engineering of Ministry of Education, Sichuan University, Chengdu 610065, China

<sup>c</sup> Max Planck Institute for Polymer Research, Ackermannweg 10, 55128 Mainz, Germany. E-mail: chenchaojian@gmail.com

† Electronic supplementary information (ESI) available. See DOI: 10.1039/d1mh01965a

‡ These authors contributed equally to this work.



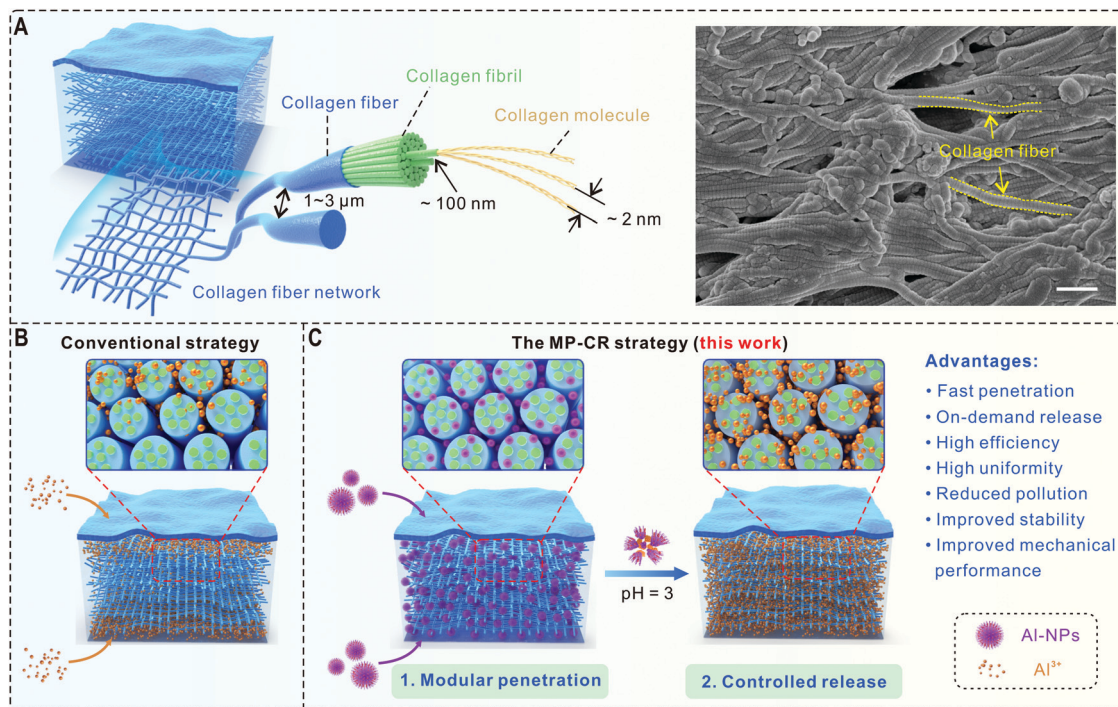


**Fig. 1** Different strategies for the internal crosslinking of hierarchical collagen fibers. (A) Schematic and SEM image showing the hierarchical structure of leather. Scale bar: 1 μm. (B) The conventional strategy of using small-molecule agents results in inefficient penetration of collagen fibers and poor uniformity. (C) The MP-CR strategy of using nanoparticles for improved internal modification of collagen fibers with high uniformity and efficiency.

As a hierarchically fibrous matrix composed of collagen molecules, leather can be regarded as an ideal model to investigate the internal modification of natural hierarchical materials. As shown in Fig. 1A, the most fundamental unit of leather is a super-coiled, right-handed triple helix structure, which is formed by three intertwined, left-handed polypeptide chains.<sup>25</sup> The collagen molecules with a typical length of ~300 nm and a diameter of ~1.5 nm are covalently cross-linked to form microfibrils, which can further organize into bundles of collagen fibers with a diameter of 100–500 nm.<sup>26</sup> The 3D network formed by interweaving and interpenetrating collagen fibers is the basic organizational structure of leather.<sup>27,28</sup> The spacings between neighboring collagen molecules, fibrils, and fibers are ~2 nm, ~100 nm, and 1–3 μm, respectively.<sup>29,30</sup> Small-molecule agents, for example, trivalent chromium ions (Cr<sup>3+</sup>)<sup>31</sup> and aluminum ions (Al<sup>3+</sup>),<sup>32</sup> have been widely used for the internal crosslinking of leather to prevent it from the negative impact by external stimuli such as sweat, moisture, microbial degradation, and heat damage.<sup>33–35</sup> However, uneven distribution of small-molecule crosslinkers and low crosslinking efficiency are usually observed in the conventional strategy (Fig. 1B).<sup>36–38</sup> These factors not only largely affect the overall performance of the products, but also bring new problems including water pollution by heavy metal ions.

Because the diffusion of small molecules in natural hierarchical materials is rarely studied, it is challenging to increase the efficiency and uniformity of the conventional strategy. In polymer sciences, size exclusion chromatography (SEC) is a leading technique to separate polymers and measure the

molecular weight distributions using a porous gel column with hierarchical pores. Smaller polymers can enter different sizes of pores and therefore stay longer in the column, while polymers with higher molecular weights only travel into bigger pores and elute faster (Fig. S1, ESI†). Inspired by the working principle of SEC, here we propose a novel two-step strategy, namely modular penetration and controlled release (MP-CR), for improving the internal crosslinking of hierarchical collagen fibers. As illustrated in Fig. 1C, we design and fabricate pH-responsive aluminum-loaded nanoparticles (Al-NPs) with an inert polymer surface. In the first step of “modular penetration”, Al-NPs do not enter small vacancies between collagen molecules due to their relatively large size. Instead, they can quickly penetrate deep into the leather matrix, behaving like large polymers in SEC columns. In the second step, the Al-NPs distributed in the collagen fiber network can be degraded and disassembled on demand by tuning the pH, resulting in the controlled release of much smaller Al<sup>3+</sup> into the nanoscale vacancies between collagen molecules. Therefore, highly uniform and effective internal crosslinking can be achieved. Remarkably, the obtained leather products show comprehensively improved mechanical properties and stability. This novel MP-CR strategy is not only suitable for leather reinforcement, but can also be extended to significantly broader areas for the internal functionalization of other natural and synthetic hierarchical materials such as hydrogels and metal–organic frameworks (MOFs). By designing and employing different functional nanoparticles, the obtained hierarchical materials will meet urgent needs in various fields such as biomedicine, catalysis, energy storage and wearable electronics.



## 2. Results and discussion

### 2.1. Fabrication and characterization of Al-NPs

To demonstrate that the MP-CR strategy is more effective for the internal modification of natural hierarchical materials, pH-responsive Al-NPs were fabricated *via in situ* mineralization using a functional terpolymer PPAAG as a template (Fig. 2A). As a proof of concept, poly(ethylene glycol)methyl ether acrylate (PEGMA,  $M_n \sim 480 \text{ g mol}^{-1}$ ), acrylic acid (AA), and acrylamide (AM) were copolymerized to synthesize terpolymer poly(PEGMA-co-AA-co-AM) (PPAA), which was then reacted with a large excess amount of glyoxal to obtain PPAAG (Fig. S2, ESI<sup>†</sup>). The carboxyl groups in PPAAG can coordinate with  $\text{Al}^{3+}$  in an aqueous solution, providing metal sources for *in situ* formation of  $\text{Al}(\text{OH})_3$  minerals under alkaline conditions. Aldehyde groups are introduced to the terpolymer due to their reactivity with amino groups, which can further enhance the internal cross-linking effect. The long PEGMA side chains of PPAAG will form the shell of Al-NPs, which ensures the nanoparticle stability and avoids the interaction between Al-NPs and collagen during the penetration. As shown in Fig. S4 (ESI<sup>†</sup>), the  $^1\text{H}$  nuclear magnetic resonance (NMR) spectrum of PPAA with important signals assigned proves the successful polymerization. After aldehyde modification, the amide peak at 6.52–7.12 ppm disappeared completely and two new peaks at 6.05 ppm and 9.42 ppm were found, confirming the successful and high-efficiency

post-functionalization. In addition, the Fourier transform infrared (FT-IR) spectrum of PPAAG in Fig. S5 (ESI<sup>†</sup>) displays the characteristic peaks of  $\text{C}=\text{O}$  at  $1632 \text{ cm}^{-1}$  and  $\text{C}-\text{H}$  at  $2924 \text{ cm}^{-1}$ , which can be ascribed to the aldehyde group, further verifying the successful synthesis of PPAAG.<sup>39,40</sup>

Subsequently, solutions of PPAAG and  $\text{AlCl}_3$  were mixed to allow the coordination of  $\text{Al}^{3+}$  with carboxyl groups. The pH was then tuned by adding dropwise a NaOH solution to induce the generation of  $\text{Al}(\text{OH})_3$  around the AA moieties. In this step, the molar ratio of  $[\text{AA}]/[\text{Al}^{3+}]/[\text{OH}^-]$  was set as 1:1:3 to ensure the complete binding of  $\text{Al}^{3+}$  to the polymer template. Aluminum-loaded nanoparticles (Al-NPs) with a mineralized core and a functional polymer shell are the result after further crystallization and self-assembly steps (Fig. 2A). The morphology and size of the Al-NPs were characterized by transmission electron microscopy (TEM) and dynamic light scattering (DLS). Spherical nanoparticles with an average size of  $21.2 \pm 4.8 \text{ nm}$  were observed in the TEM image (Fig. 2B). However, the average diameter determined by DLS is  $92.6 \pm 0.5 \text{ nm}$  (Fig. 2C). The size difference can be partially ascribed to the presence of a hydrated polymer shell on the nanoparticle surface in solution, while TEM images of the nanoparticles were collected in the dry state. In addition, multi-core nanoparticles may also be present, which can make the average diameter significantly larger. We further employed energy dispersive X-ray spectrometry (EDX) and X-ray diffraction (XRD) to analyze the core composition. As shown in Fig. 2D, the

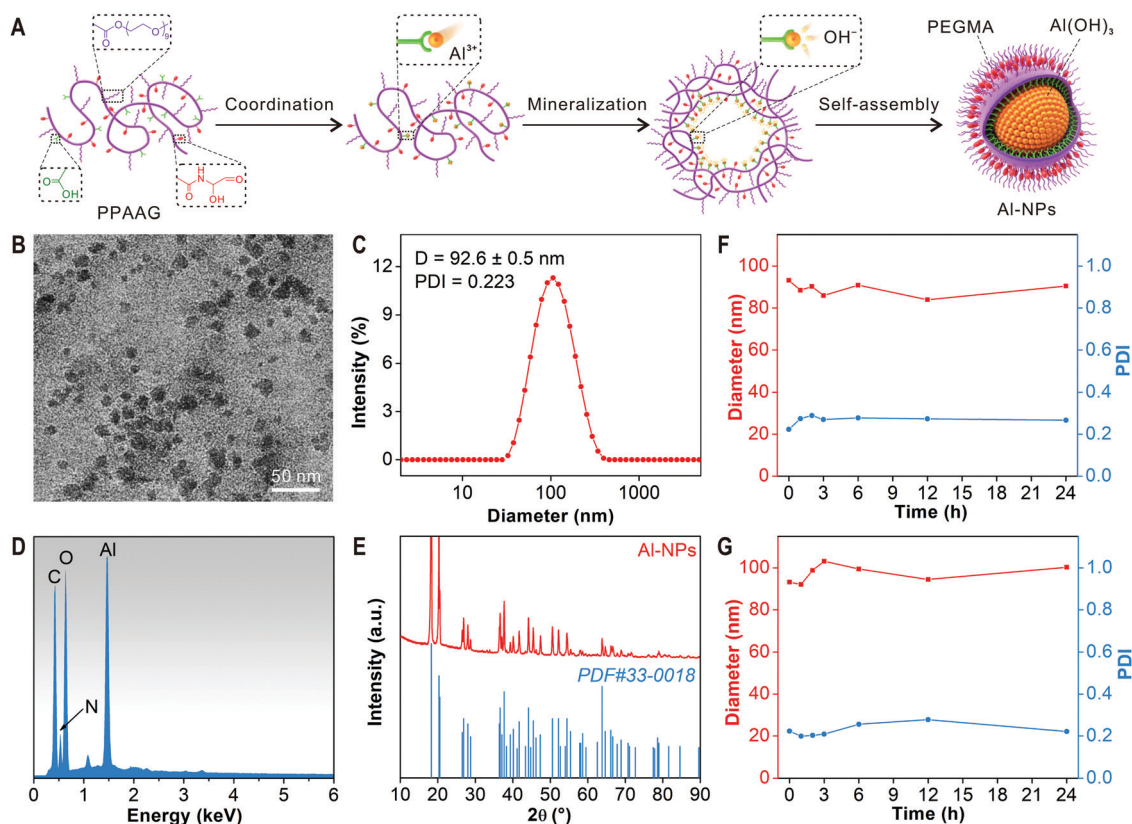


Fig. 2 Fabrication and characterization of Al-NPs. (A) Schematic illustration of the procedure for preparing Al-NPs *via in situ* mineralization using terpolymer PPAAG as a template. (B) TEM image, (C) DLS size distribution, and (D) EDX spectrum of Al-NPs. (E) XRD patterns of Al-NPs and PDF#33-0018. (F and G) Stability test for Al-NPs in an aqueous solution of 1000 mM NaCl (F) or 5 mg mL<sup>-1</sup> BSA (G) over 24 h.



EDX spectrum clearly shows characteristic peaks of Al and O elements from  $\text{Al}(\text{OH})_3$ . Moreover, the XRD pattern of Al-NPs in Fig. 2E fits with a hexagonal phase of nanocrystalline  $\text{Al}(\text{OH})_3$  (PDF#33-0018).<sup>41</sup> Collectively, the above results confirm the successful preparation of Al-NPs using PPAAG as a template. In addition, the  $\text{Al}^{3+}$  loading efficiency was determined as 87.8% by an established method as described in the ESI.†

To test the MP-CR strategy, it is important that the Al-NPs can keep their nanosized structure intact during the penetration process. Therefore, we examined the stability of Al-NPs under high concentrations of NaCl (1000 mM) and bovine serum albumin (BSA, 5 mg mL<sup>-1</sup>), which are more extreme conditions than the internal environment of collagen fibers. The size and polydispersity index (PDI) of the Al-NPs tracked by DLS did not show obvious changes over 24 h (Fig. 2F and G). These results indicate the high stability of Al-NPs, which can be attributed to the excellent protection by the hydrated PEGMA shell.<sup>42,43</sup>

For comparison, we also prepared nanoparticles without glyoxal modification as a control. The sample templated by PPAA was named Al-NPs(PPAA) and characterized by TEM and DLS (Fig. S6, ESI†). Spherical nanoparticles with an average diameter of  $19.4 \pm 5.4$  nm were observed in the TEM image (Fig. S6A, ESI†). Meanwhile, the average size determined by DLS

is  $79.2 \pm 0.3$  nm (Fig. S6B, ESI†). The particle size difference between Al-NPs ( $92.6 \pm 0.5$  nm) and Al-NPs(PPAA) might be attributed to the introduction of aldehyde groups. Fig. S6C–F (ESI†) show that Al-NPs(PPAA) have the same elemental composition and crystal structure and a similar stability compared with Al-NPs.

## 2.2. Modular penetration and pH-controlled release of Al-NPs

To achieve the “controlled release” of  $\text{Al}^{3+}$  in the second step of MP-CR, we examined the pH-sensitivity of the Al-NPs in solution. The size changes of the nanoparticles under various pH values from 3 to 5 and 7 were detected by DLS (Fig. 3A). In addition, we also studied the  $\text{Al}^{3+}$  release behavior under these conditions by inductively coupled plasma atomic emission spectroscopy (ICP-AES) (Fig. 3B). Under pH 5 and 7, it is obvious that the size of the Al-NPs did not change and the cumulative release of  $\text{Al}^{3+}$  was negligible. However, the average size of Al-NPs drastically increased from  $\sim 90$  nm to  $>1500$  nm when the pH was adjusted to 3 after 3 h. Under this condition, the compact nanoparticles degraded and the hydrophilic–hydrophobic balance of the polymer hybrid was changed. Therefore, the remaining polymeric structures became loose and aggregated to larger assemblies. Meanwhile, the cumulative release of  $\text{Al}^{3+}$  also

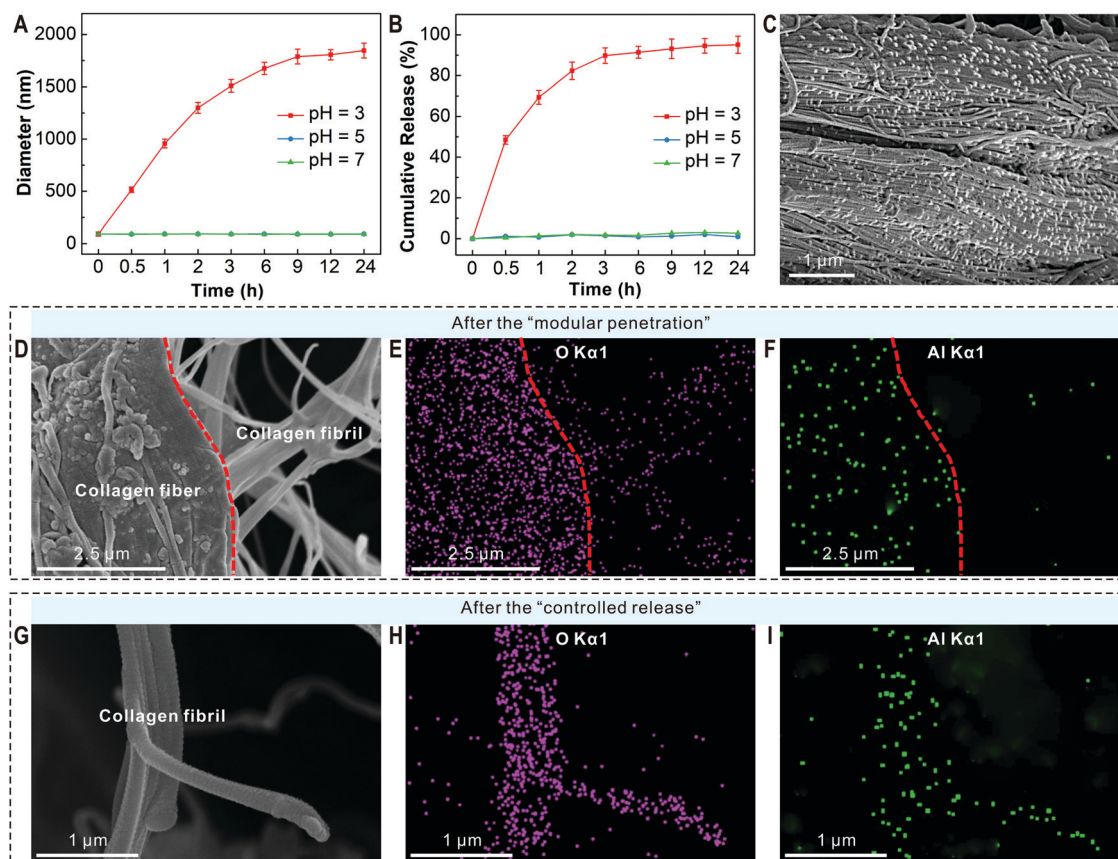


Fig. 3 Modular penetration and pH-controlled release of the Al-NPs. (A) Size changes and (B)  $\text{Al}^{3+}$  release behaviors of the Al-NPs in aqueous solutions with different pH values from 3 to 5 and 7 over 24 h. (C) The SEM image showing the distribution of Al-NPs in the cross-section of leather after modular penetration. (D–F) SEM image and EDX elemental maps displaying the oxygen and aluminum distributions after the first step of molecular penetration. (G–I) Oxygen and aluminum distributions in the collagen fibrils after the disassembly and degradation of the Al-NPs.



displayed a rapid increase under pH 3, with  $\sim 90\%$  of  $\text{Al}^{3+}$  released in 3 h. These data demonstrate that the Al-NPs can be disassembled under pH 3, leading to controlled release of  $\text{Al}^{3+}$ .

Encouraged by their pH-sensitivity and good stability under different conditions, we then investigated the nanoparticle penetration and  $\text{Al}^{3+}$  release of Al-NPs in natural hierarchical materials using leather as a model. As mentioned above, the leather matrix possesses different scales of vacancies between collagen molecules, microfibrils, and fibers (Fig. 1A). To elucidate the mechanism of MP-CR, we first compared the diffusion behaviors of Al-NPs and a conventional small-molecule crosslinker  $\text{Al}_2(\text{SO}_4)_3$  in leather. A non-crosslinking agent  $\text{K}_2\text{SO}_4$  was used as a control. Specifically, we treated several pieces of pickled sheep skin with these metal-containing agents for 30 min and 1 h. The molar amounts of metals used for different groups were the same. After freeze-drying, the samples were sliced, and the cross-sectional metal distribution was analyzed by EDX. As shown in Fig. S7A and B (ESI<sup>†</sup>), the leather samples treated by  $\text{Al}_2(\text{SO}_4)_3$  demonstrated uneven metal distribution, with obviously lower amounts of Al in the middle area than in both side layers (grain side and fresh side). Surprisingly, the leather tanned with Al-NPs displayed a much more uniform distribution of Al after treating for only 30 min (Fig. S7C, ESI<sup>†</sup>). In addition, we can see evenly distributed nanoparticles in the cross-sectional SEM image of the sheep skin treated with the Al-NPs (Fig. 3C). These results not only confirm the good stability of the nanoparticles during the process, but also clearly reveal that nano-sized particles can penetrate faster and deeper into collagen fibers. These counterintuitive phenomena can be ascribed to the following two reasons: (1) the Al-NPs enter only into relatively large pores in leather due to their nanoscale dimension, exhibiting similar behavior to high-molecular-weight polymers in SEC columns; (2) the inert PEGMA shell of Al-NPs can prevent their interaction with collagen during penetration, while reactive trivalent  $\text{Al}^{3+}$  can be easily bound by collagen molecules in the surface layers.

To further prove the reasons and elucidate MP-CR's mechanism, we employed SEM and EDX to track in more detail the aluminum and oxygen distributions at different levels of the structures (collagen fibers and fibrils) after the penetration. As shown in Fig. 3D, we can clearly see the distribution of nanoparticles on the collagen fibers on the left, while the collagen fibrils in the right half of the SEM image look very smooth (see Fig. S8 for more details, ESI<sup>†</sup>), preliminarily indicating that the Al-NPs did not enter the nanoscale spacings between collagen molecules. Additionally, the EDX elemental map in Fig. 3E shows that O element can be detected in both areas. However, Al element is only distributed in the collagen fibers (left) and the signal from the right side is negligible (Fig. 3F). This clearly proves that the Al-NPs only penetrated the relatively large vacancies in collagen fibers and could not enter the interior of the collagen fibrils. The second reason has been further verified by comparison to the diffusion behavior of  $\text{K}_2\text{SO}_4$ . As shown in Fig. S7E and F (ESI<sup>†</sup>), monovalent metal ion  $\text{K}^+$  with a comparable size to  $\text{Al}^{3+}$  but weaker interaction with collagen can diffuse easier in leather, and thus more uniform distribution was detected.

After the modular penetration of Al-NPs into the collagen fiber network, it is important that the reactive crosslinkers can be released to further diffuse into the nanoscale vacancies between collagen molecules. Therefore, the leather treated by Al-NPs was immersed into a dilute  $\text{H}_2\text{SO}_4$  solution (pH = 3) for 2 h. The sample was then characterized by SEM (Fig. 3G) and EDX elemental mapping (Fig. 3H and I). We can now see overlapping distributions of O and Al elements on the collagen fibrils, indicating the successful disassembly of the Al-NPs upon pH change and penetration of  $\text{Al}^{3+}$  into the interior of the collagen fibrils. This is because  $\text{Al}^{3+}$  with a significantly reduced size is the only possible source of Al that can penetrate collagen fibrils.

### 2.3. Internal reinforcement of leather with pH-responsive Al-NPs

The above results have extensively elucidated the mechanism of the MP-CR strategy by demonstrating its two-step modular penetration and controlled release process. Therefore, we believe that using responsive nanoparticles is a superior method for the internal modification of natural hierarchical materials compared to traditional approaches of using small-molecule agents. As a proof of concept, we compared the internal crosslinking effects on leather by applying different tanning agents, which include the small-molecule crosslinker  $\text{Al}_2(\text{SO}_4)_3$ , the pH-responsive Al-NPs templated by terpolymer PPAAG, and a mixture of  $\text{Al}_2(\text{SO}_4)_3$  and PPAAG (named Al&PPAAG). Meanwhile, pH-responsive Al-NPs(PPAA) templated by terpolymer PPAA was used as a control to determine the impact of aldehyde groups on the internal crosslinking of leather. Fig. 4A displays the flow chart for leather treatment with the Al-NPs. The corresponding procedures of using  $\text{Al}_2(\text{SO}_4)_3$ , Al&PPAAG, and Al-NPs(PPAA) are also summarized in Fig. S9 (ESI<sup>†</sup>).

The Al-NPs penetrated into the leather matrix were treated with dilute  $\text{H}_2\text{SO}_4$  (pH = 3) for 2 h to trigger nanoparticle degradation and disassembly, resulting in the release of trivalent  $\text{Al}^{3+}$  and functional PPAAG into the interstices of the collagen fibrils and molecules. The interior pH of the matrix was then tuned to 3.8, which allowed the coordination of  $\text{Al}^{3+}$  with carboxyl groups from collagen molecules and PPAAG. In the next step, we further increased the pH to 8.0. Under these conditions, the aldehyde groups ( $-\text{CHO}$ ) in PPAAG bonded with the amino groups ( $-\text{NH}_2$ ) on the collagen surfaces through a Schiff base reaction, leading to synergistic crosslinking *via* supramolecular metal coordination and covalent reaction (Fig. S10, ESI<sup>†</sup>).

To check the internal crosslinking effect, SEM was employed to observe the cross-sectional morphology of the leather tanned by different agents. The fiber bundles in the samples treated with Al-NPs and Al&PPAAG both show good dispersion with noticeable spacing between fibers (Fig. 4B and C). However, the collagen fibers in the leather tanned by  $\text{Al}_2(\text{SO}_4)_3$  display obvious aggregation and clustering, while the spacings between different bundles are significantly larger (Fig. 4D). The difference can be attributed to the presence of PPAAG in the first two agents, which can serve as a relatively long linker between different fibers based on the Schiff base reaction. In addition, we compared the cross-sectional distribution of Al for the



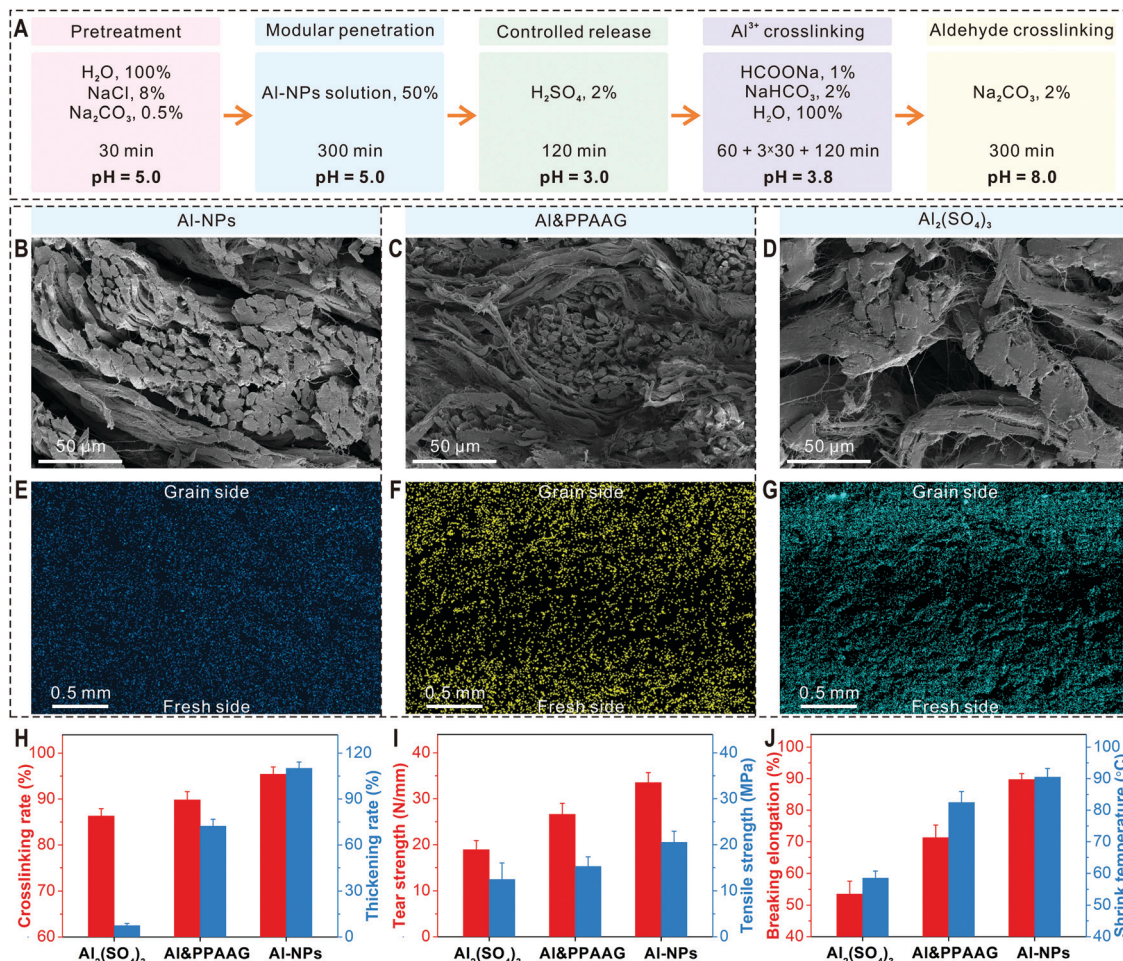


**Fig. 4** Smart Al-NPs for the internal reinforcement of leather. (A) The flow chart for the internal crosslinking of leather using pH-responsive multifunctional Al-NPs. The dosage of agents used was compared to the weight of the limed skin, which was set as 100%. During the Al<sup>3+</sup> crosslinking step, the pH value of the reaction system was adjusted to 3.8 by adding 1% sodium formate for 60 min and 2% NaHCO<sub>3</sub> three times at 30 min intervals, after which the reaction was heated to 40 °C for 120 min and then soaked in the crosslinking solution overnight. (B–G) Cross-sectional SEM images and EDX elemental maps of the leather samples cross-linked by different agents: (B and E) Al-NPs; (C and F) AI&PPAAG, and (D and G) 2% Al<sub>2</sub>(SO<sub>4</sub>)<sub>3</sub>. (H–J) Comparison of various properties and parameters of the leather samples cross-linked by Al<sub>2</sub>(SO<sub>4</sub>)<sub>3</sub>, AI&PPAAG, and Al-NPs: (H) the crosslinking rate of Al<sup>3+</sup> and thickening rate, (I) tear strength and tensile strength, and (J) breaking elongation and shrinkage temperature.

samples after standard tanning procedures. Owing to the nano-size effect, a very uniform Al distribution was observed for the leather treated with Al-NPs (Fig. 4E). However, Al<sup>3+</sup> from both AI&PPAAG and Al<sub>2</sub>(SO<sub>4</sub>)<sub>3</sub> could not efficiently diffuse into the central part of the leather, resulting in uneven distributions (Fig. 4F and G). These results clearly reveal that the responsive Al-NPs can be used to enhance the uniformity during the internal modification of leather.

Significantly, the MP-CR strategy can also increase the usage/crosslinking efficiency of metal ions. As shown in Fig. 4H, the Al<sup>3+</sup> crosslinking rate for leather samples treated with the three tanning agents, Al<sub>2</sub>(SO<sub>4</sub>)<sub>3</sub>, AI&PPAAG, and Al-NPs, gradually increased from 86.3% to 89.8% and 95.4%, which indicates that both the functional PPAAG and the nano-size of Al-NPs contributed to the efficiency improvement. These results also imply that MP-CR is a more environmentally friendly strategy. Comparing the use of Al-NPs with conventional small-molecule Al<sub>2</sub>(SO<sub>4</sub>)<sub>3</sub>, the metal ions left in wastewater significantly dropped

from 13.7% to 4.6%, showing remarkable potential of MP-CR for reducing water pollution by metal ions. In addition, we also measured the thickening rate of the samples. This is an important indicator for the filling characteristics of crosslinking agents and the fullness of leather products. Similarly, the leather treated with Al-NPs showed huge rises in the thickening rate compared with those tanned by AI&PPAAG and Al<sub>2</sub>(SO<sub>4</sub>)<sub>3</sub>, being 37.8% and 102.6%, respectively (Fig. 4H).

Most importantly, the MP-CR strategy using responsive nanoparticles can comprehensively improve the mechanical performance and stability of the treated leather. As a proof of concept, we tested various mechanical properties of the tanned samples, including the tear strength, tensile strength, and breaking elongation. Before measurement, all samples were further treated by a standard fatliquoring technique, and the details are provided in Fig. S11 (ESI<sup>†</sup>). This is a process of treating leather with oil or other fatliquoring agents, which can improve the physical and mechanical properties, making the



leather products easier to use and suitable for testing. As shown in Fig. 4I and J, the leather sample treated with Al-NPs demonstrated the best performance among the three groups in all the tested properties. It should be emphasized that all these improvements come from two important features of the Al-NPs: (1) the use of functional terpolymer PPAAG as a template not only assisted the formation and stabilization of nanoparticles, but also provided additional connections between collagen molecules; (2) the nano-size effect of Al-NPs significantly enhanced the uniformity and effectiveness of Al<sup>3+</sup> penetration. Particularly for the breaking elongation, the leather sample treated with Al-NPs showed a tremendous increase compared to the other two groups, confirming again the profound effect of the MP-CR strategy. Finally, we measured the shrinkage temperature ( $T_s$ ) of different samples to compare their hydrothermal stability (Fig. 4J). Although the addition of PPAAG to the conventional small-molecule crosslinker increased the  $T_s$  by >20 °C, the use of Al-NPs further largely raised the  $T_s$  to 90.5°, showing that the MP-CR strategy can also obviously improve the hydrothermal stability of leather. It can be seen from Fig. S12 (ESI†) that the Al<sup>3+</sup> crosslinking rates of Al-NPs(PPAA) without aldehyde groups and Al-NPs are almost the same. This can be attributed to the similar MP-CR effect of the two nanoparticles. However, other properties such as the thickening rate, tensile strength and shrinkage temperature of leather crosslinked by Al-NPs are higher than those of leather samples treated by Al-NPs(PPAA), which can be ascribed to the additional crosslinking with aldehyde groups.

### 3. Conclusions

In summary, MP-CR is a novel and superior strategy for the internal modification of hierarchical materials with high efficiency and uniformity. Different from conventional strategies based on small molecules, MP-CR uses responsive nanoparticles to deliver and release reactive crosslinkers. By comparing the diffusion of mineralized Al-NPs and small molecules in collagen fiber networks, we have elucidated the MP-CR's mechanism, and demonstrated its unique two-step modular penetration and controlled release process. Due to their nano-size effect and inert surface, the Al-NPs only travel into relatively large pores, and therefore can penetrate faster and deeper into the hierarchical network. After on-demand pH-controlled degradation and disassembly, the released crosslinking agents further diffuse into nanoscale vacancies between the collagen molecules, leading to more effective and even internal crosslinking. Remarkably, the products treated by the MP-CR strategy reveal comprehensively improved mechanical properties and stability. Meanwhile, the water pollution caused by heavy metal ions in conventional processing can be tremendously reduced. In principle, this strategy is compatible with different functional nanoparticles, and it should be applicable to reinforce and functionalize other natural and synthetic hierarchical materials including hydrogels, MOFs and MXene films for various emerging applications in biomedicine, catalysis, energy storage and wearable electronics.

### Conflicts of interest

There are no conflicts of interest to declare.

### Acknowledgements

This study was supported by the Key Technology Support Program of Sichuan Province (2021YFG0241), Opening Project of Key Laboratory of Leather Chemistry and Engineering of Ministry of Education, Sichuan University (SCU2021D005), and the Program of Sichuan University featured research groups in engineering disciplines. The authors also thank Zhonghui Wang for the assistance with some experiments. Open Access funding provided by the Max Planck Society.

### References

- 1 R. Lakes, Materials with structural hierarchy, *Nature*, 1993, **361**, 511–515.
- 2 P. Fratzl and R. Weinkamer, Nature's hierarchical materials, *Prog. Mater. Sci.*, 2007, **52**, 1263–1334.
- 3 S. Ling, D. L. Kaplan and M. J. Buehler, Nanofibrils in nature and materials engineering, *Nat. Rev. Mater.*, 2018, **3**, 18016.
- 4 F. J. Martin-Martinez, K. Jin, D. L. Barreiro and M. J. Buehler, The Rise of Hierarchical Nanostructured Materials from Renewable Sources: Learning from Nature, *ACS Nano*, 2018, **12**, 7425–7433.
- 5 S. Ling, *et al.*, Biopolymer nanofibrils: Structure, modeling, preparation, and applications, *Prog. Polym. Sci.*, 2018, **85**, 1–56.
- 6 C. Chen, D. Y. W. Ng and T. Weil, Polymer bioconjugates: Modern design concepts toward precision hybrid materials, *Prog. Polym. Sci.*, 2020, **105**, 101241.
- 7 R. J. Moon, A. Martini, J. Nairn, J. Simonsen and J. Youngblood, Cellulose nanomaterials review: structure, properties and nanocomposites, *Chem. Soc. Rev.*, 2011, **40**, 3941–3994.
- 8 F. G. Omenetto and D. L. Kaplan, New Opportunities for an Ancient Material, *Science*, 2010, **329**, 528–531.
- 9 C. Chen, *et al.*, Structure-property-function relationships of natural and engineered wood, *Nat. Rev. Mater.*, 2020, **5**, 642–666.
- 10 S. Keten, Z. Xu, B. Ihle and M. J. Buehler, Nanoconfinement controls stiffness, strength and mechanical toughness of beta-sheet crystals in silk, *Nat. Mater.*, 2010, **9**, 359–367.
- 11 X. Peng, *et al.*, A breathable, biodegradable, antibacterial, and self-powered electronic skin based on all-nanofiber triboelectric nanogenerators, *Sci. Adv.*, 2020, **6**, eaba9624.
- 12 A. Miyamoto, *et al.*, Inflammation-free, gas-permeable, lightweight, stretchable on-skin electronics with nano-meshes, *Nat. Nanotechnol.*, 2017, **12**, 907–913.
- 13 P. Tseng, *et al.*, Directed assembly of bio-inspired hierarchical materials with controlled nanofibrillar architectures, *Nat. Nanotechnol.*, 2017, **12**, 474–480.



- 14 Y. Pei, L. Wang, K. Tang and D. L. Kaplan, Biopolymer Nanoscale Assemblies as Building Blocks for New Materials: A Review, *Adv. Funct. Mater.*, 2021, **31**, 2008552.
- 15 T. Li, *et al.*, Developing fibrillated cellulose as a sustainable technological material, *Nature*, 2021, **590**, 47–56.
- 16 C. Xu, *et al.*, Nature-inspired hierarchical materials for sensing and energy storage applications, *Chem. Soc. Rev.*, 2021, **50**, 4856–4871.
- 17 M. Diab and T. Mokari, Bioinspired Hierarchical Porous Structures for Engineering Advanced Functional Inorganic Materials, *Adv. Mater.*, 2018, **30**, 1706349.
- 18 Y. Liu, K. He, G. Chen, W. R. Leow and X. Chen, Nature-Inspired Structural Materials for Flexible Electronic Devices, *Chem. Rev.*, 2017, **117**, 12893–12941.
- 19 L. Wang, D. Chen, K. Jiang and G. Shen, New insights and perspectives into biological materials for flexible electronics, *Chem. Soc. Rev.*, 2017, **46**, 6764–6815.
- 20 L. Dai, *et al.*, Ultrasensitive physical, Bio, and chemical sensors derived from 1-, 2-, and 3-D nanocellulosic materials, *Small*, 2020, **16**, 1906567.
- 21 J. Song, *et al.*, Processing bulk natural wood into a high-performance structural material, *Nature*, 2018, **554**, 224–228.
- 22 S. Wan, *et al.*, High-strength scalable MXene films through bridging-induced densification, *Science*, 2021, **374**, 96–99.
- 23 Q. Liu and I. I. Smalyukh, Liquid crystalline cellulose-based nematogels, *Sci. Adv.*, 2017, **3**, e1700981.
- 24 X. Wang, *et al.*, Hierarchically structured C@SnO<sub>2</sub>@C nanofiber bundles with high stability and effective ambipolar diffusion kinetics for high-performance Li-ion batteries, *J. Mater. Chem. A*, 2016, **4**, 18783–18791.
- 25 D. Hulmes, J.-C. Jesior, A. Miller, C. Berthet-Colominas and C. Wolff, Electron microscopy shows periodic structure in collagen fibril cross sections, *Proc. Natl. Acad. Sci. U. S. A.*, 1981, **78**, 3567–3571.
- 26 A. Gautieri, S. Vesentini, A. Redaelli and M. J. Buehler, Hierarchical Structure and Nanomechanics of Collagen Microfibrils from the Atomistic Scale Up, *Nano Lett.*, 2011, **11**, 757–766.
- 27 Z. C. Jiang, *et al.*, A 'Trojan horse strategy' for the development of a renewable leather tanning agent produced via an AlCl<sub>3</sub>-catalyzed cellulose depolymerization, *Green Chem.*, 2020, **22**, 316–321.
- 28 X. Liu, Y. Wang, X. Wang and H. Jiang, Development of hyperbranched poly-(amine-ester) based aldehyde/chrome-free tanning agents for sustainable leather resource recycling, *Green Chem.*, 2021, **23**, 5924–5935.
- 29 J. P. Orgel, T. C. Irving, A. Miller and T. J. Wess, Microfibrillar structure of type I collagen in situ, *Proc. Natl. Acad. Sci. U. S. A.*, 2006, **103**, 9001–9005.
- 30 E. A. Abou Néel, *et al.*, Collagen—emerging collagen based therapies hit the patient, *Adv. Drug Delivery Rev.*, 2013, **65**, 429–456.
- 31 R. Zhu, *et al.*, A smart high chrome exhaustion and chrome-less tanning system based on chromium (III)-loaded nanoparticles for cleaner leather processing, *J. Cleaner Prod.*, 2020, **277**, 123278.
- 32 D. Gao, *et al.*, An eco-friendly approach for leather manufacture based on P(POSS-MAA)-aluminum tanning agent combination tannage, *J. Cleaner Prod.*, 2020, **257**, 120546.
- 33 V. John Sundar, A. Gnanamani, C. Muralidharan, N. K. Chandrababu and A. B. Mandal, Recovery and utilization of proteinous wastes of leather making: a review, *Rev. Environ. Sci. Bio/Technol.*, 2010, **10**, 151–163.
- 34 Q. Xia, *et al.*, Chromium Cross-Linking Based Immobilization of Silver Nanoparticle Coating on Leather Surface with Broad-Spectrum Antimicrobial Activity and Durability, *ACS Appl. Mater. Interfaces*, 2019, **11**, 2352–2363.
- 35 Z. Jiang, *et al.*, A 'Trojan horse strategy' for the development of a renewable leather tanning agent produced via an AlCl<sub>3</sub>-catalyzed cellulose depolymerization, *Green Chem.*, 2020, **22**, 316–321.
- 36 M. Sathish, A. Dhathathreyan and J. R. Rao, Ultraefficient Tanning Process: Role of Mass Transfer Efficiency and Sorption Kinetics of Cr(III) in Leather Processing, *ACS Sustainable Chem. Eng.*, 2019, **7**, 3875–3882.
- 37 Z. Jiang, *et al.*, Selective degradation and oxidation of hemicellulose in corncob to oligosaccharides: From biomass into masking agent for sustainable leather tanning, *J. Hazard. Mater.*, 2021, **413**, 125425.
- 38 Z. Jiang, *et al.*, On the development of chrome-free tanning agents: an advanced Trojan horse strategy using 'Al-Zr-oligosaccharides' produced by the depolymerization and oxidation of biomass, *Green Chem.*, 2021, **23**, 2640–2651.
- 39 G. Zeng, *et al.*, Enhancement of Cd(II) adsorption by polyacrylic acid modified magnetic mesoporous carbon, *Chem. Eng. J.*, 2015, **259**, 153–160.
- 40 V. Folliard, *et al.*, Oxidative coupling of a mixture of bioalcohols to produce a more sustainable acrolein: An in depth look in the mechanism implying aldehydes co-adsorption and acid/base sites, *Appl. Catal., B*, 2020, **268**, 118421.
- 41 J. B. Zhou, S. L. Yang, J. G. Yu and Z. Shu, Novel hollow microspheres of hierarchical zinc-aluminum layered double hydroxides and their enhanced adsorption capacity for phosphate in water, *J. Hazard. Mater.*, 2011, **192**, 1114–1121.
- 42 B. Pelaz, *et al.*, Surface Functionalization of Nanoparticles with Polyethylene Glycol: Effects on Protein Adsorption and Cellular Uptake, *ACS Nano*, 2015, **9**, 6996–7008.
- 43 H. Otsuka, Y. Nagasaki and K. Kataoka, PEGylated nanoparticles for biological and pharmaceutical applications, *Adv. Drug Delivery Rev.*, 2012, **64**, 246–255.

